Received: 24 December 2020 | Revised: 25 March 2021 | Accepted: 27 March 2021

DOI: 10.1002/mrc.5157

SPECIAL ISSUE RESEARCH ARTICLE

WILEY

# Validation of temperature-controlled rheo-MRI measurements in a submillimeter-gap Couette geometry

**Klaudia W. Milc**[1] | **Maria R. Serial**[1] | **John Philippi**[1] | **Joshua A. Dijksman**[2] | **John P. M. van Duynhoven**[1,3] | **Camilla Terenzi**[1]

[1]Laboratory of Biophysics, Wageningen University, Wageningen, The Netherlands

[2]Laboratory of Physical Chemistry and Soft Matter, Wageningen University, Wageningen, The Netherlands

[3]Science and Technology, Unilever Foods Innovation Centre Hive, Wageningen, The Netherlands

**Correspondence**
John P. M. van Duynhoven, Laboratory of Biophysics, Wageningen University, Stippeneng 4, Wageningen 6708, The Netherlands.
Email: john.vanduynhoven@wur.nl

**Funding information**
4TU Precision Medicine Program; Bruker BioSpin

**Abstract**

A temperature-controlled submillimeter-gap (500 μm) rheo-magnetic resonance imaging (MRI) Couette cell has been developed to measure confined flow of soft structured materials under controlled temperature. The proposed setup enables performing rheo-MRI measurements using (i) a spatially uniform temperature control over the range 15°C to 40°C and (ii) a high spatial resolution up to 10 μm, as a consequence of the improved mechanical stability of the in-house developed rotating elements. Here, we demonstrate the performance of the cell for the rheo-MRI velocimetry study of a thixotropic fat crystal dispersion, a complex fluid commonly used in food manufacturing. The submillimeter-gap geometry and variable temperature capability of the cell enable observing the effects of shear- and temperature-induced fat recrystallization on both wall slip and shear banding under strongly confined flow. Our improved rheo-MRI setup opens new perspectives for the fundamental study of strongly confined flow, cooperative effects, and the underlying interparticle interactions and for ultimately aiding optimization of products involved in spreading/extrusion, such as cosmetics and foods.

**KEYWORDS**

$^{1}$H rheo-MRI, confined flow, food microstructure, temperature control

## 1 | INTRODUCTION

Industrially relevant complex fluids, such as food dispersions or emulsion-based cosmetics and paints, flow through geometries that drastically vary in size during manufacturing or even customer use. In factories, pipes used for transporting such fluids between different process modules have diameters of meters/centimeters, whereas millimeter-/micrometer-sized nozzles are typically used for extrusion of fluids into molds and packaging. Flow in millimeter-sized gaps is also present during mastication and spreading of foods, governing mouthfeel and customer satisfaction. Additionally, flow through micron-scale geometries is encountered in many novel technologies, such as microflow reactors and 3D printing in food or chemical industry. Most structured fluids used in those processes, such as food colloids or polymer gels, exhibit a microstructure with length scales in the order of tens or hundreds of micrometers and flow through gaps whose sizes are comparable with these

structural length scales. In such conditions, flow can be considered as strongly confined and can differ from nonconfined flow as a result of interparticle interactions.

Currently, standard rheology focuses mostly on bulk studies of nonconfined flow of complex fluids.[1] Recent developments in the combination of rheology with molecular spectroscopy and/or imaging techniques have boosted our molecular-level understanding of nonconfined flow, in relation with shear-induced microstructural rearrangements, even in complex fluids. For instance, rheo-magnetic resonance imaging (rheo-MRI)[2] enables detecting shear-induced structural changes, such as alignment[3] or network destruction or rejuvenation,[4] that occur at micrometer/millimeter scales, whereas rheo-small-angle X-ray diffraction (rheo-SAXD) offers insight into changes, for example, in terms of the sizes of the structural elements, that occur at a submicron scale.[4,5] However, as has been demonstrated for emulsions[6] and granular media,[7] strongly confined flow properties cannot be inferred from measurements carried out in nonconfined conditions. When the confinement size, $d$, becomes comparable with the characteristic length scale of the fluid's microstructure, $l$, namely, when $d \leq 100 \cdot l$, flow can become cooperative and, thus, spatially heterogeneous.[6] Flow cooperativity is driven by nonlocal effects, where the local relation between stress and strain rate at a given location within the fluid can be strongly influenced by the plastic rearrangements occurring at a neighboring location, as illustrated in Figure 1.[6,8]

To quantitatively describe spatially heterogeneous cooperative flow in soft structured dispersions, experimental flow setups are needed that enable velocimetry measurements in submillimeter gaps with high spatial resolution.[2c,9] Currently available methods for high-resolution microfluidic flow measurements, for example, particle image velocimetry (PIV)[6,10] or dynamic light scattering (DLS),[11] are not suitable for applications to most complex fluids, such as optically opaque and strongly scattering materials. Additionally, these methods often require the use of tracer particles, which in turn may alter the interparticle interactions responsible for cooperative flow.

Rheo-MRI velocimetry,[12] already widely applied to room-temperature flow studies of complex fluids, does not suffer from any of the above-mentioned limitations.[2a,b,13] Yet, so far, only geometries with 1- to 4-mm gap sizes have been available, which are unsuitable for probing confinement effects in most food colloids due to (i) the excessively large gap size compared with the relevant structural lengths and (ii) the nonnegligible stress inhomogeneity throughout the gap, which in turn hampers the identification of cooperativity or other complex flow properties. The lack of geometries with submillimeter gap sizes is due to several challenges associated with their implementation in rheo-MRI setups. The first challenge is the low signal-to-noise ratio (SNR) in submillimeter geometries, due to both small sample volumes and the need to increase the MRI spatial resolution in order to acquire enough data points within the submillimeter gap. Achieving high MRI resolution is, in turn, hampered by the second challenge, namely, the off-axis mechanical displacement of the bob during rotation. The so-called bob wobble is a well-known severe issue of rotating concentric cylindrical setups in general,[14] including the currently available rheo-MRI geometries. Such wobbling limits the achievable spatial resolution typically to only about 50 μm, not sufficient for submillimeter geometries, and causes unstable shear flow as well as a fluctuating gap size during shear.[15]

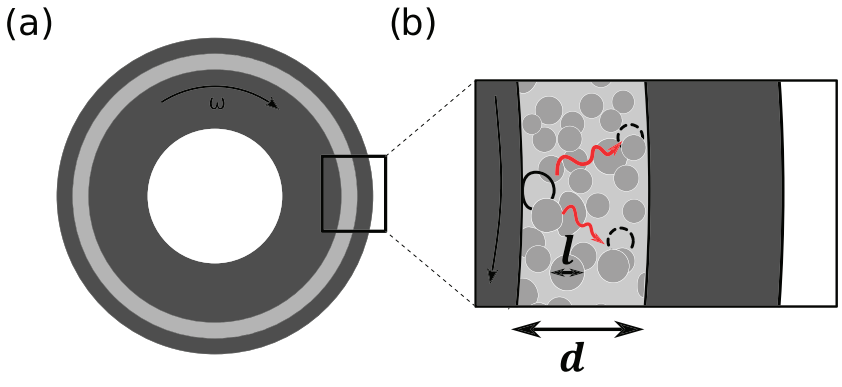


**FIGURE 1** Schematic representation of a complex fluid, with particles of average diameter $l$, being sheared in a Couette cell (CC) made of polyether ether ketone (PEEK) (dark gray) with gap size $d$. (a) Top view of the CC; cup filled with the complex fluid (light gray) and bob filled with a reference fluid (white). (b) Zoom-in of a gap-filling fluid exhibiting cooperative flow: when $d \leq 100 \cdot l$, plastic rearrangements (empty black circles) of particles can cause stress modulations throughout the gap (red arrows) resulting in additional correlated plastic rearrangements at neighboring sites (dashed black circles)

Due to both its inherent complex phenomenology and the lack of versatile submillimeter flow setups, cooperativity is still poorly understood at the fundamental level and not yet quantified with a unique model. Additionally, not all fluids undergoing strongly confined flow exhibit cooperativity effects, while for some other fluids, such as polymer microgels,[16] these effects were observed even for the particle size to confinement ratio, $d/l \geq 100$.[17] Hence, despite its profound influence on bulk flow, for example, in terms of suppressing local yield stress,[18] cooperativity cannot yet be taken into account in the industrial design and manufacturing of foods, paints, or other complex fluids, thus limiting the ability to correctly predict the microstructural and rheological properties of the final products. An additional key factor to be taken into account when optimizing manufacturing of most complex fluids, such as fat or fiber dispersions,[19] polymer solutions,[20] granular media,[7] or concentrated suspensions,[21] is temperature. The latter determines the microstructure, in terms of crystal form and particle sizes, as well as the viscosity of the final products. It is thus desirable to have highly controlled temperature conditions during flow and to be able to quantify flow behavior and cooperativity effects as a function of temperature. The temperature ranges most commonly used during manufacturing vary depending on the industry and the flowing fluid. For production and design of foods, it is particularly important to study the effect of temperatures in the range 10°C to 80°C. At these temperatures, microstructure-formation processes take place, such as gelation, crystallization, or dissolution.[22] Studies of the effect of body temperature on flow of fluids are also important for customer-oriented food design. To this goal, a few temperature-controlled shear Couette cells (CCs) with millimeter-sized gaps have been constructed and used in rheo-NMR spectroscopy, and small-angle scattering (SAS) experiments.[23] However, up to date, temperature-controlled rheo-MRI velocimetric studies have not yet been carried out.

In the present work, we extend the well-established advantages of rheo-MRI towards temperature-controlled studies of strongly confined flow of complex fluids, such as food dispersions or emulsions with particles larger than 10 μm, by developing and validating a temperature-controlled rheo-MRI CC with a gap size of 500 μm. We first demonstrate the key technical improvements in our proposed submillimeter-gap CC for rheo-MRI, namely, (i) the high mechanical stability of the bob, which enables imposing steady shear flow and measuring local velocity profiles with MRI spatial resolution up to 10 μm, and (ii) the spatially uniform temperature control over 15°C to 45°C, which enables the study of confined flow as a function of temperature. Thereafter, we show an illustrative application of the submillimeter-gap CC for studies of confined flow in a fat crystal dispersion (FCD) at 15°C and 30°C.

## 2 | IMPROVED DESIGN OF THE SUBMILLIMETER-GAP RHEO-MRI CC

Our proposed design for a submillimeter-gap rheo-MRI CC is shown in Figure 2. For its use in high-field NMR spectrometers, the cell is made of polyether ether ketone (PEEK), like all other available rheo-MRI geometries. The bob contains an internal chamber that can be filled with a reference Newtonian fluid. Both cup and bob have smooth walls that can be modified by sandblasting or serration. For all experiments, the cup is filled with a sample, and upon insertion of the bob, the sample is enclosed within a gap of 500 μm. For improving the off-axis mechanical stability during rotation, the bob has been designed as one piece, and the bearing has been extended further down into the cup to better fix the axis of rotation. In the commercially available millimeter-gap rheo-MRI geometries, the bob is made as a two-piece element with a separate top, and the bearing is shorter by 5 mm as compared with our new design: both factors make the millimeter-gap setups less mechanically stable in the off-axis direction. In addition, in our new submillimeter-gap CC, the casing of the cup houses a water circuit that can be connected to an external water bath operating at bath temperatures, $T_b \sim 15$°C to 45°C, with which the sample temperature, $T_s$, can be controlled during shear. The upper temperature limit of 45°C in this design is dictated by the highest temperature that the glue used in construction of the cell can withstand. As PEEK can

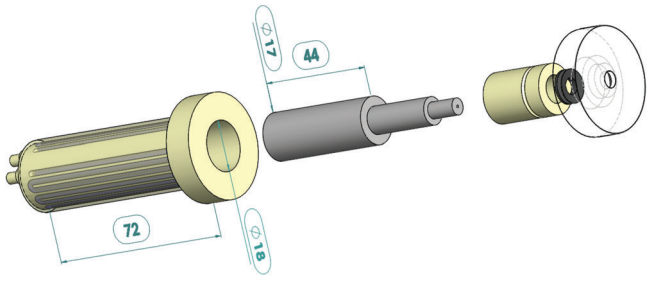


FIGURE 2 Technical drawing of the submillimeter-gap rheo-MRI Couette cell (CC) made of polyether ether ketone (PEEK). From left to right: cup with the temperature control water circuit, the bob, and the bearing. All dimensions are in millimeter. The outer shield of the cup and the top part of the bearing are made semitransparent in the figure for visibility of the water circuit and of the rubber o-ring, respectively. The design of the cell and the technical drawing were done in SolidWorks 2018

withstand up to 170°C, the current temperature limit could be extended by using an appropriately heat-resistant glue. Similarly to the commercially available rheo-MRI setups, the assembly of the cell prohibits shear stress measurements inside the MRI spectrometer. However, the whole cell is replicated to also fit into a standard cup holder for Anton Paar rheometers for torque measurements, and the bob can be used with a commercially available custom shaft holder.[15]

## 3 | MATERIALS AND METHODS

### 3.1 | Sample preparation

Micronized fat crystals, prepared as described elsewhere,[4] were added to a commercial sunflower oil in a 3:8 (w/w) ratio, and the blend was heated to 50°C to erase crystal polymorphic history. The mixture was cooled to 20°C at a rate of 0.2°C $min^{-1}$. The obtained FCD contained polydispersed spherulitic fat crystallite aggregates with diameter of approximately 150 μm. The sample was used for measurements within 8 h from the crystallization.

### 3.2 | Rheo-NMR/-MRI measurements

All MRI and rheo-MRI experiments were performed on a wide-bore Bruker Avance III spectrometer operating at 7 T. Excitation and detection of the $^1$H signal was performed with a birdcage radiofrequency coil with an inner diameter of 25 mm, in the standard microimaging gradient system Micro 2.5 (Bruker) with maximum gradient intensity of 1.5 T $m^{-1}$ along all three axes. For rheo-MRI measurements, the Bruker rheo-MRI accessory was used in combination with the custom-made 500-μm-gap CC or the commercially available serrated CC with $r_i/r_o = 7/11$ mm (4-mm gap), also made of PEEK.

$^1$H rheo-MRI measurements aiming at assessing the mechanical stability of the bob were performed with the cup and bob filled with distilled water doped with 1 wt% $CuSO_4$ (Merck), to decrease the NMR longitudinal relaxation time of water to about 20 ms. The decreased relaxation time enabled us to use a short repetition time, $T_R = 14$ ms, and low number of scans while retaining a high SNR. As a result, the duration of one scan was minimized to 7 s, as required for the scopes of this set of measurements. For the acquisition of images under the constant rotation of the bob at 0.72 rpm, fast low-angle shot (FLASH) MRI sequence was used with a slice selective sinc excitation pulse of duration 1 ms and tip angle of 30°. The field of view (FOV) was 20 × 20 mm, and the resulting spatial resolution was 40 × 40 μm/pixel. Consecutive images were acquired over three axial slices, each 1 mm thick, at heights $z = 8$, 16, and 22 mm from the bottom of the bob. Acquisition of each image lasted 7 s; therefore, to measure over two rotations of the bob (167 s), 25 images were acquired. The position of the center of the cup and that of the bob were extracted from each image using a circle tracking algorithm in MATLAB R2018b that enables subpixel accuracy in the centroid estimation. The coordinates of the two centers were subtracted from each other to yield the positions of the bob's center with respect to the cup's center in consecutive images.

$^1$H chemical shift imaging (CSI) NMR measurements of $CH_3OH$ (Merck, purity > 99%) filling both the cup and the bob were conducted to calibrate the temperature over the range $T_b = 15$°C to 45°C in steps of 5°C. CSI spectra from three axial slices, 1 mm thick each, at heights $z = 18$, 26, and 32 mm from the bottom of the cup were recorded with a FOV of 25.6 × 25.6 mm and the resolution of 40 × 40 μm/pixel. The local temperature in each pixel, $T_{loc}$, was calculated from the difference in chemical shift ($\Delta\delta$) between the $CH_3$ and the OH methanol peaks using the following equation[24]:

$$T_{loc}[^\circ C] = 135.85 - 36.54 \cdot \Delta\delta - 21.85 \cdot \Delta\delta^2. \quad (1)$$

The in situ sample temperature, $T_s^{MRI}$, was calculated by averaging values of $T_{loc}$ within and over the three slices. The bulk, ex situ, temperature of the sample inside the cup, $T_s^{TC}$, was measured with a thermocouple.

One-dimensional velocity profiles were measured by a pulsed gradient spin echo (PGSE) sequence with a slice thickness of 1 mm in two dimensions,[25] echo time $T_E = 19.5$ ms, and $T_R = 2$ s. The duration of the velocity-encoding gradient pulses and their interpulse spacing were $\delta = 1$ ms and $\Delta = 13$ ms, respectively. The amplitudes of the velocity-encoding gradients were, respectively, in the 500-μm-gap and 4-mm-gap CC, set to (i) 1.50, 1.19, and 0.14 T $m^{-1}$ for recording shear rates of $\dot{\gamma} = 0.5, 1,$ and $8\ s^{-1}$ or to (ii) 0.51 and 0.05 T $m^{-1}$ for recording shear rates of $\dot{\gamma} = 0.5$ and $8\ s^{-1}$. To avoid chemical shift artifacts, a chemical shift selective (CHESS) suppression module, as implemented by Serial et al.,[26] was used in all measurements using three 90° chemically selective pulses with bandwidth of 0.8 kHz. The offset was set to 1 or 0.1 kHz, respectively, for measurements at shear rates of $\dot{\gamma} = 0.5$ and $8\ s^{-1}$ at room temperature or at shear rate of $\dot{\gamma} = 1\ s^{-1}$ under variable temperature conditions. Different offsets were used due to the presence of water in the water channels giving rise to an additional MR signal, thus altering the spectrometer's reference frequency in the temperature-controlled studies. The

frequency-encoding read gradient provided a 10-mm-long slice over 1024 pixels, such that the spatial resolution was $\Delta x = 10$ μm. The time needed to obtain a single velocity profile within the gap was 34 min for a number of scans of $NS = 512$. Three replicate measurements were collected at each rotation speed.

## 4 | RESULTS AND DISCUSSION

### 4.1 | Mechanical stability of the bob

Our previous measurement of the off-axis displacement of the bob in a commercially available 1-mm rheo-MRI CC yielded wobbling values up to ~60–80 μm at low rotation rates, where wobbling is most significant (data not reported here). Such wobbling size would be excessive in our submillimeter-gap setup, resulting in ~16% variation in the gap size during rheo-MRI measurements. Furthermore, during the off-axis movement of the bob under shear, the sheared fluid is pushed sideways within the gap, thus resulting in additional artifactual flow components. The consequent distortions that appear in the velocity profiles hamper the analysis of the underlying "true" flow behavior, thus making the identification of flow effects such as cooperativity even more challenging. COMSOL simulations of the effect of the off-axis displacement by 80 μm on the expected linear velocity profiles of a Newtonian fluid flowing in a 500-μm-gap CC (data not shown here) yield up to 50% deviation from the expected linear velocity. If the off-axis displacement is reduced down to about 10 μm, such deviation becomes only 5%, which is within the experimental error associated with rheo-MRI flow measurements. Such improved off-axis mechanical stability also enables achieving a spatial MRI resolution of 10 μm with the 500-μm CC, which in turn is desired to record the velocity profiles with a sufficient number of data points. Hence, reducing the off-axis wobble to below 10 μm is of importance for both (i) minimizing the artifacts in the velocity profiles and (ii) avoiding having to discard pixels close to the bob because of the wobbling. Below, we set out to quantify the improvement in the mechanical stability achieved in our newly designed submillimeter-gap cell.

Figure 3 shows $^1$H MRI FLASH measurements along both $x$ and $y$ directions of the off-axis displacement of the center of the bob, filled with doped water, with respect to the center of the cup, expressed as a percentage of the gap size $d$. As indicated in the figure, the movement of the bob was tracked at three positions along the bob's height ($z$ axis). In all three slices, the maximum observed off-axis displacement was within 5% of the gap size and appeared linearly decreasing when going from top to bottom, respectively, being equal to 25, 17.5, and 7.5 μm at $z = 8$, 16, and 22 mm. The error associated with the wobble values, due to the limit of accuracy in the estimation of the bob's and the cup's centers by the circle tracking algorithm, is ±1 μm at all heights. The lower off-axis wobbling towards the bottom of the bob is due to the fact that (i) the protrusion that fits within the well at the bottom of the cup locally fixes the axis of rotation and (ii) the probe is fixed at its base but exhibits mechanical instability in the top part, where it also connects to the shaft and the forces acting on it are the largest.

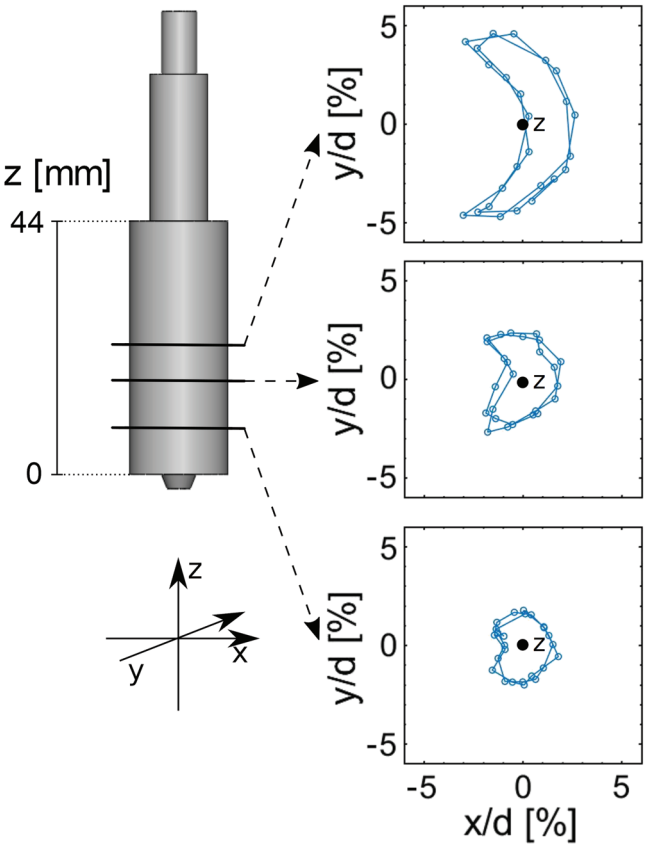


**FIGURE 3** Rheo-MRI measurements of the off-axis displacement of the bob, filled with doped water, during rotation at 0.72 rpm. Consecutive fast low-angle shot (FLASH) images of 1-mm-thick axial slices were measured. Twenty-five images with the duration time of 7 s each were acquired to track two full rotations. The position of the center of the bob was extracted from each image using a circle tracking algorithm in MATLAB R2018b. Plots on the right show the coordinates obtained from slices measured at $z = 8$, 16, and 22 mm along the bob's height, respectively

The achieved reduction in the off-axis displacement down to 7.5 μm ($z = 8$ mm) corresponds to a 10-fold improvement in stability as compared with commercially available rheo-MRI CC and, importantly, is below the desired MRI spatial resolution of 10 μm for acquiring velocity profiles in submillimeter-gap geometries.

This remarkable improvement in off-axis mechanical stability enables us to use the cell for applying a steady and unidirectional shear and for obtaining artifact-free velocity profiles even at low shear rates ($\dot{\gamma}$). We believe that the mechanical stability of our rheo-MRI setup can be enhanced even further by improving the stability of the MRI probe head. Based on the observations in Figure 3, we decided to record all our velocity profiles at $z = 10$ mm, where the off-axis displacement and its error can be estimated from the linear fit of the measured wobble values as $(9.5 \pm 2)$ μm. This position is optimal considering both the stability of the bob and the SNR, which is highest closest to the center of the coil ($z = 14$ mm).

## 4.2 | Calibration of the temperature control circuit

All applications of temperature-controlled flow studies, for example, involving crystallization, gelation, or polymerization processes, require highly stable and uniform temperature control. Temperature fluctuations can, for instance, lead to inhomogeneities in the sample and/or to flow instabilities.

In this work, we have calibrated the temperature of the submillimeter-gap CC at seven nominal bath temperature ($T_b$) values over the range 15°C to 45°C. The temperature was estimated both locally ($T_{loc}$), from spatially resolved $^1$H CSI spectra of a methanol-filled CC by using Equation 1,[24] and as bulk value ($T_s^{TC}$ and $T_s^{MRI}$), respectively, ex situ using a thermocouple or in situ by averaging the $T_{loc}$ values obtained by $^1$H CSI for all pixels from the three selected slices.

Figure 4a shows the temperature maps obtained from the CSI measurements, recorded at $T_b = 45$°C. It can be seen that the temperature is uniform within each slice and across the $z$-range examined. A similar observation was obtained for all other $T_b$ values. Thus, an in situ temperature calibration curve could be constructed, averaging the local sample temperature, $T_{loc}$, within and over the three slices. Figure 4b shows the ex situ and in situ calibration curves, both evidencing a linear dependence of the temperature inside the gap. The standard deviation for the ex situ and in situ temperature values is 0.3°C and 1°C, respectively, mostly due to imperfect shimming typical of wide-bore magnets. The expected temperature fluctuation is estimated to be 0.3°C, based on the fluctuations of the thermostat of the water bath. The embedding of such temperature circuit in the cell enables carrying out rheo-MRI experiments at controlled uniform temperatures within the range $T_s = 16$°C to 40°C. This introduces a significant advancement to rheo-MRI, so far mostly limited to room-temperature studies.

## 4.3 | Case study: Local flow behavior of a FCD

As an illustrative application of our novel submillimeter-gap rheo-MRI CC, we studied the confined flow behavior of a FCD, with 27% fat concentration. FCDs are used in production of fat-based products, such as chocolate or

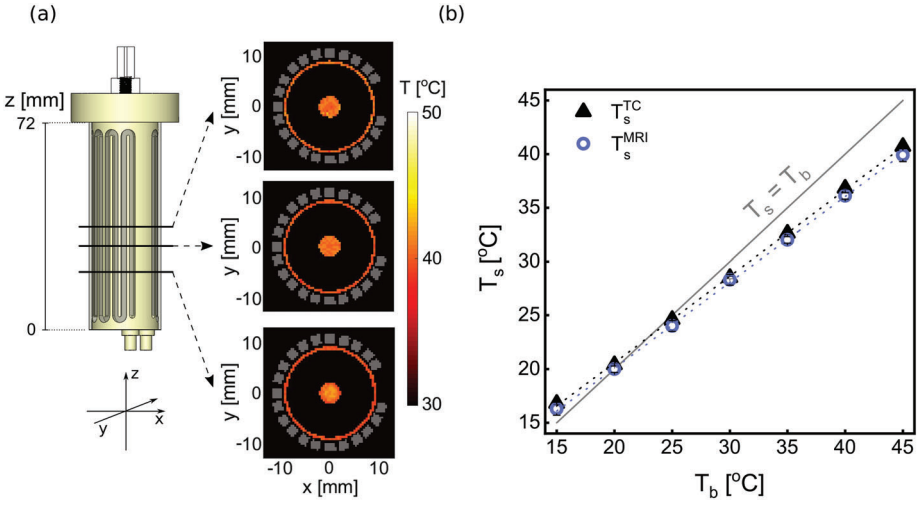


**FIGURE 4** Calibrations of the temperature circuit (water channels shown in gray both in the drawing of the cell and in the images), with the cup and the bob filled with $CH_3OH$. (a) At $T_b = 45$°C: axial $^1$H MR chemical shift imaging (CSI) images acquired for three slices, each 1 mm thick, at positions $z = 18$, 26, and 32 mm along the cell's height, showing a uniform temperature, $T_{loc}$, as calculated using Equation 1.[24] (b) At $T_b = 15$°C to 45°C: effective bulk temperature in the gap, measured ex situ with a thermocouple ($T_s^{TC}$) and also in situ by $^1$H MR CSI ($T_s^{MRI}$) by averaging the $T_{loc}$ values obtained for the three axial slices shown in (a)

margarine. Due to the presence of large crystal aggregates with sizes up to $l = 200\ \mu m$, FCDs are prone to exhibit nontrivial and strongly temperature-dependent flow behavior in submillimeter- or millimeter-sized confinements.[9a,19a]

We have first carried out a preliminary investigation of the global flow behavior of the FCD by rheology, at shear rates in the range $\dot{\gamma} = 0.01 - 100\,s^{-1}$, as commonly done to identify shear rates at which flow becomes unstable.[2c] From these measurements (data not reported here), we could observe flow instabilities at and below $\dot{\gamma} = 1\,s^{-1}$. Therefore, we performed rheo-MRI measurements at shear rates above ($\dot{\gamma} = 8\,s^{-1}$) or below ($\dot{\gamma} = 0.5\,s^{-1}$) the transition from unstable to stable flow regimes and compared the results obtained in the 500-μm-gap and 4-mm-gap CCs. We note that the percentage stress variation across the 500-μm-gap CC, calculated as the ratio of stresses at the outer and inner wall, is only 11%,[27] which yields linear velocity profiles in the absence of flow instabilities. Hence, flow instabilities can be easily observed from velocity profiles acquired with the submillimeter-gap CC. Instead, in millimeter-gap CCs, the nonnegligible stress distribution > 20% may make it impossible to discern and quantify possible effects due to flow cooperativity. Figure 5 shows the comparison between the 1D velocity profiles of the FCD at applied shear rates of $\dot{\gamma} = 0.5$ and $8\,s^{-1}$ in the (a) 500-μm-gap and (b) 4-mm-gap CC. All measured velocity profiles are compared with the calculated velocity profiles expected for a simple yield-stress fluid in the absence of cooperativity effects. In both geometries, wall slip was quantified by an extrapolation of the last 10 pixels at the outer wall, and subtracted from the velocity profiles, as done in previous work.[2c] Figure 5a shows that in the submillimeter-gap CC, flow of the FCD is linear at $\dot{\gamma} = 8\,s^{-1}$, with an expected nearly uniform shear rate throughout the gap. In the unstable flow regime, at $\dot{\gamma} = 0.5\,s^{-1}$, a strongly curved velocity profile is observed, suggesting a spatially dependent viscosity as also observed in cooperative flow.[2c] In Figure 5b, the experimental velocity profiles for the 4-mm-gap CC appear concave at both applied shear rates. The corresponding predicted velocity profiles for a fluid that does not exhibit cooperativity displays the same deviation from linearity as experimentally observed for the FCD. This significant effect is solely due to the expected dominant stress variation across the 4-mm-gap CC, which in turn makes it impossible to easily unravel flow cooperativity.

For the same FCD sample, we set out to illustrate the importance of temperature-controlled submillimeter rheo-MRI studies. Due to the crystalline nature of the platelets that form the aggregates in the FCD, flow at a temperature higher than room temperature was studied to unravel the influence of recrystallization effects on strongly confined flow. In Figure 6a,b, the flow behavior at $\dot{\gamma} = 1\,s^{-1}$ of the 27% FCD is shown at $T_b = 15°C$ and 30°C, respectively, at three shearing times over a 1.5-h time span.

At $T_b$°=°15°C, the confined flow is stable, likely indicating no significant shear-induced recrystallization effects. Concave velocity profiles evidence a nonuniform effective shear rate in agreement with observations at ambient temperature and low shear rate (see Figure 5). In addition, localized flow measurement enabled the

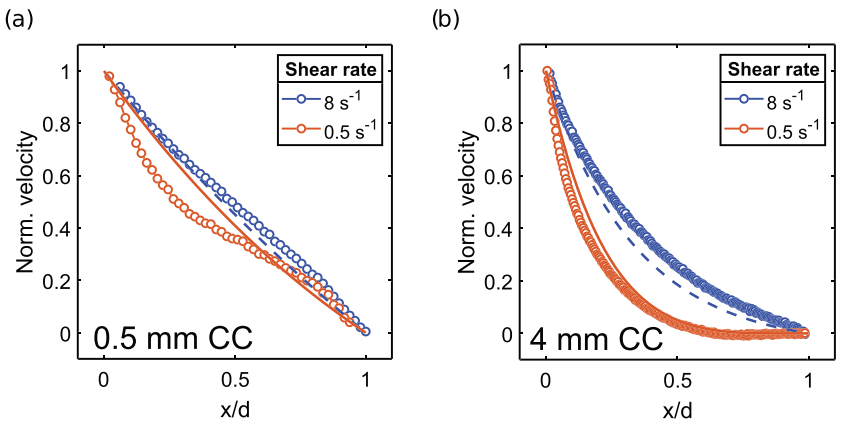


**FIGURE 5** Experimental $^1$H rheo-MRI velocity profiles (open circles) of a 27% fat crystal dispersion (FCD), measured in (a) 500-μm-gap Couette cell (CC) with smooth walls and (b) 4-mm-gap CC with serrated walls, at $\dot{\gamma} = 8$ and $0.5\,s^{-1}$, compared with calculated velocity profiles (dashed and solid lines, respectively) of Herschel–Bulkley yield-stress fluid ($4 + 2.54\dot{\gamma}^{0.5}$) without nonlocal effects, in the respective geometries. At both shear rates, velocities were normalized to the respective maximum velocity. Measured flow profiles were corrected for slippage at the outer wall, by subtracting the slip velocity determined by extrapolation of the last 10 pixels. Slip velocities at the outer wall as a percentage of the maximum expected velocity were 9% and 20% in the 500-μm-gap CC and 5% and 10% for the 4-mm-gap CC, at high and low $\dot{\gamma}$, respectively

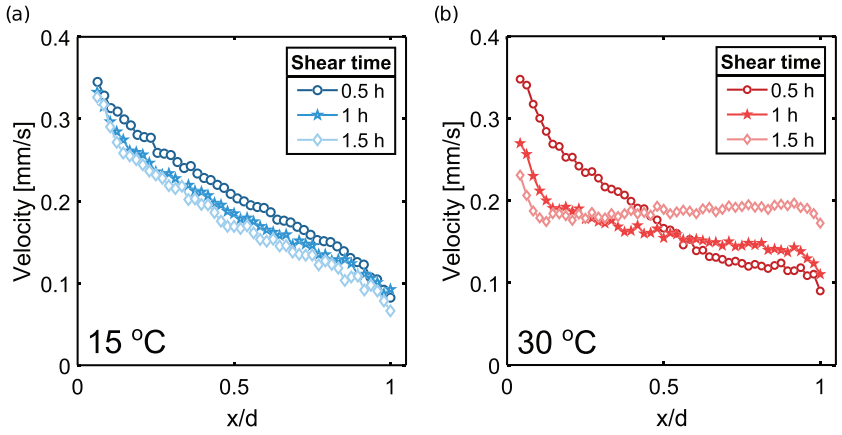


**FIGURE 6** Dependence on shearing time (0.5, 1, and 1.5 h) of $^1$H rheo-MRI velocity profiles for a 27% fat crystal dispersion (FCD), measured at $\dot{\gamma} = 1\,s^{-1}$ and at (a) $T_b = 15°C$ or (b) $T_b = 30°C$. The flow profiles were acquired consecutively under continuous shear. The duration of each experiment was 0.5 h, with the resulting flow profile being an average measurement over such experiment time

quantification of a constant slip at both cell walls of (20° ± 3)%. The flow behavior of the dispersion at $T_b = 30°C$ appears drastically different. The flow exhibits a significant wall slip during the first hour of shearing, with progressively decreasing shear banding effects. In the final 0.5 h, no discrete shear bands could be further distinguished. This indicates that recrystallization takes place, which weakens the structure of the material causing it to become more susceptible to shear in the final 0.5 h. Additionally, recrystallization results in the formation of larger aggregates, which likely induces cooperativity effects, because a concave, rather than a linear profile, is observed in the final 0.5 h. We note that the demonstrated uniformity and stability of the temperature control circuit enables ruling out any possible effect due to temperature fluctuations.

The presence of cooperativity effects in the rheo-MRI results displayed in Figures 5 and 6 can be confirmed and quantified by fitting the spatially resolved velocities in combination with rheological stress measurements.[28] This requires separate measurements of bulk and spatially resolved flow in twin setups.[6,17b,18,29] For reliable quantitative velocimetry studies, the spatially resolved flow profiles must be recorded at high spatial resolution and high SNR, while minimizing mechanical instability artifacts. From Figures 5a and 6, it can be seen that such requirements are satisfied with our improved rheo-MRI setup. Thanks to the enhanced off-axis mechanical stability of the bob, acquired velocity profiles are free from wobble artifacts and acquired with very high MRI spatial resolution of 10 μm/pixel. The SNR obtained in the 500-μm-gap CC is 120 ± 5, as given by the ratio of mean signal intensity to the standard deviation of the noise, which is comparable with that of wider gap geometries.[15,30] Here, modeling the confined flow behavior of the FCD would have required accounting for the observed microstructural rearrangements and temperature effects, which was beyond the scope of this work.

## 5 | CONCLUSIONS

With the aim to study strongly confined flow by rheo-MRI, we have developed a 500-μm-gap rheo-MRI CC, which requires small sample volumes (∼0.4 ml) and is equipped with a water circuit for temperature control in the range 15°C to 40°C. Calibration of the water circuit over this operational temperature range was obtained by performing $^1$H CSI measurements of the cell filled with methanol, where the difference in chemical shift between $CH_3$ and OH signals can be used to quantify sample temperature. This approach revealed a spatially homogeneous temperature, within ±0.3°C, over the entire sample volume. The mechanical stability of the rotating bob was improved by a factor of ∼10 with respect to currently available rheo-MRI setups. The MRI spatial resolution could thus be boosted up to ∼10 μm, the latter value being the estimated reduced size of off-axis wobbling of the bob. All these improved rheo-MRI features were conjointly exploited here to study the temperature-dependent confined flow of a thixotropic FCD sample. By using the submillimeter-gap CC, evidences could be observed for (i) the onset of nonuniform flow, suggesting cooperativity effects at low shear rate and room temperature not discernible in wider gaps, and for (ii) shear-induced microstructural changes at 30°C, not visible at room temperature and linked to recrystallization effects. We foresee that our improved rheo-MRI setup, suitable for studying strongly confined flow, is a powerful tool for enabling fundamental studies of cooperative flow under in situ or in operando conditions and, ultimately, for aiding the rational design of foods, or other soft particulate dispersions such as emulsion-based paints or polymer coatings.

## ACKNOWLEDGEMENTS

We thank Bruker BioSpin (Germany) for cosponsoring this project and Dieter Gross and Thomas Oerther from

Bruker BioSpin for useful discussions on the rheo-MRI setup. We also thank Ruud den Adel (Unilever) for preparation and useful discussion on FCD. C.T. acknowledges funding from the 4TU Precision Medicine Program supported by High Tech for a Sustainable Future (https://www.4tu.nl/en/news/!/393/awarding_hightech/).

## PEER REVIEW

The peer review history for this article is available at https://publons.com/publon/10.1002/mrc.5157.

## ORCID

*Klaudia W. Milc* https://orcid.org/0000-0002-2657-3654
*Maria R. Serial* https://orcid.org/0000-0003-3052-4916
*Joshua A. Dijksman* https://orcid.org/0000-0002-8337-1434
*John P. M. van Duynhoven* https://orcid.org/0000-0001-9769-0113
*Camilla Terenzi* https://orcid.org/0000-0003-3278-026X

## REFERENCES

[1] P. Fischer, E. J. Windhab, *Curr. Opin. Colloid Interface Sci.* **2011**, *16*, 36.
[2] a) P. Galvosas, T. I. Brox, S. Kuczera, *Magn. Reson. Chem.* **2019**, *57*, 757; b) P. Coussot, *Exp. Fluids* **2020**, *61*, 207; c) D. W. de Kort, S. J. Veen, H. Van As, D. Bonn, K. P. Velikov, J. P. M. van Duynhoven, *Soft Matter* **2016**, *12*, 4739.
[3] a) T. I. Brox, B. Douglass, P. Galvosas, J. R. Brown, *J. Rheol.* **2016**, *60*, 973; b) R. N. Al-kaby, J. S. Jayaratne, T. I. Brox, S. L. Codd, J. D. Seymour, J. R. Brown, *J. Rheol.* **2018**, *62*, 1125.
[4] T. Nikolaeva, R. den Adel, E. Velichko, W. G. Bouwman, D. Hermida-Merino, H. Van As, A. Voda, J. P. M. van Duynhoven, *Food Funct.* **2018**, *9*, 2102.
[5] T. Nikolaeva, R. den Adel, R. van der Sman, K. J. A. Martens, H. Van As, A. Voda, J. P. M. van Duynhoven, *Langmuir* **2019**, *35*, 2221.
[6] J. Goyon, A. Colin, L. Bocquet, *Soft Matter* **2010**, *6*, 2668.
[7] K. Kamrin, *Front. Phys.* **2019**, *7*, 1.
[8] L. Bocquet, A. Colin, A. Ajdari, *Phys. Rev. Lett.* **2009**, *103*, 036001.
[9] a) R. Campos, A. G. Marangoni, *Cryst. Growth Des.* **2014**, *14*, 1199; b) A. Rohart, J.-M. Sieffermann, C. Michon, *Colloids Surf., A* **2015**, *475*, 94.
[10] J. G. Santiago, S. T. Wereley, C. D. Meinhart, D. J. Beebe, R. J. Adrian, *Exp. Fluids* **1998**, *25*, 316.
[11] J. B. Salmon, L. Bécu, S. Manneville, A. Colin, *Eur. Phys. J. E: Soft Matter Biol. Phys.* **2003**, *10*, 209.
[12] P. T. Callaghan, *Curr. Opin. Colloid Interface Sci.* **2006**, *11*, 13.
[13] K. G. Hollingsworth, M. L. Johns, *J. Rheol.* **2004**, *48*, 787.
[14] C. W. Macosko, *Rheology: Principles, Measurements, and Applications*, Wiley **1994** 188.
[15] T. Nikolaeva, F. J. Vergeldt, R. Serial, J. A. Dijksman, P. Venema, A. Voda, J. P. M. van Duynhoven, H. Van As, *Anal. Chem.* **2020**, *92*, 4193.
[16] B. Geraud, L. Bocquet, C. Barentin, *Eur. Phys. J. E: Soft Matter Biol. Phys.* **2013**, *36*, 1.
[17] a) S. P. Meeker, R. T. Bonnecaze, M. Cloitre, *J. Rheol.* **2004**, *48*, 1295; b) L. Derzsi, D. Filippi, G. Mistura, M. Pierno, M. Lulli, M. Sbragaglia, M. Bernaschi, P. Garstecki, *Phys. Rev. E* **2017**, *95*, 052602; c) D. E. V. Andrade, M. Ferrari, P. Coussot, *J. Non-Newtonian Fluid Mech.* **2020**, *279*, 104261.
[18] J. Paredes, N. Shahidzadeh, D. Bonn, *Phys. Rev. E* **2015**, *92*, 042313.
[19] a) N. C. Acevedo, J. M. Block, A. G. Marangoni, *Faraday Discuss.* **2012**, *158*, 171; b) T. Tran, S. Ghosh, D. Rousseau, *Cryst. Growth Des.* **2014**, *14*, 6383; c) D. Klemm, B. Heublein, H.-P. Fink, A. Bohn, *Angew. Chem., Int. Ed.* **2005**, *44*, 3358.
[20] H. Mohammadigoushki, S. J. Muller, *Soft Matter* **2016**, *12*, 1051.
[21] B. K. Aral, D. M. Kalyon, *J. Rheol.* **1994**, *38*, 957.
[22] a) S. Banerjee, S. Bhattacharya, *Critical Reviews in Food Science and Nutrition* **2012**, *52*, 334; b) K. Mishra, D. Dufour, E. J. Windhab, *Cryst. Growth Des.* **2020**, *20*, 1292; c) P. R. Ramel, R. Campos, A. G. Marangoni, *Cryst. Growth Des.* **2018**, *18*, 1002.
[23] a) E. Velichko, B. Tian, T. Nikolaeva, J. Koning, J. P. M. van Duynhoven, W. G. Bouwman, *Colloids Surf., A* **2019**, *566*, 21; b) E. Laryea, N. Schuhardt, G. Guthausen, T. Oerther, M. Kind, *Microporous Mesoporous Mater.* **2018**, *269*, 65.
[24] C. Ammann, P. Meier, A. Merbach, *J. Magn. Reson.* **1982**, *46*, 319.
[25] P. T. Callaghan, *Rep. Prog. Phys.* **1999**, *62*, 599.
[26] M. R. Serial, T. Nikolaeva, F. J. Vergeldt, J. P. M. van Duynhoven, H. Van As, *Magn. Reson. Chem.* **2019**, *57*, 766.
[27] D. W. de Kort, T. Nikolaeva, J. A. Dijksman, in *Modern Magnetic Resonance*, (Ed: G. A. Webb), Springer International Publishing **2018** 1.
[28] J. Goyon, A. Colin, G. Ovarlez, A. Ajdari, L. Bocquet, *Nature* **2008**, *454*, 84.
[29] P. Jop, V. Mansard, P. Chaudhuri, L. Bocquet, A. Colin, *Phys. Rev. Lett.* **2012**, *108*, 148301.
[30] G. Ovarlez, S. Rodts, A. Ragouilliaux, P. Coussot, J. Goyon, A. Colin, *Phys. Rev. E* **2008**, *78*, 036307.

**How to cite this article:** Milc KW, Serial MR, Philippi J, Dijksman JA, van Duynhoven JPM, Terenzi C. Validation of temperature-controlled rheo-MRI measurements in a submillimeter-gap Couette geometry. *Magn Reson Chem*. 2021;1–9. https://doi.org/10.1002/mrc.5157